Multiple input multiple output experimental aeroelastic control using a receptance-based method

Bilal Mokrani[*], Francesco Palazzo[†], John E Mottershead[‡] and Sebastiano Fichera[§]

University of Liverpool, Liverpool, England L69 GH, United Kingdom

This paper presents the first experimental study of Multiple-Input Multiple-Output active vibration suppression by pole placement using the receptance method. The research is based on a purpose-built modular flexible wing equipped with leading- and trailing-edge control surfaces and two displacement sensors for measuring its position. The MIMO controller has the advantage of being designed entirely on frequency response functions, measured between the control surfaces position (control inputs) and the structural displacements (outputs), and including the actuator dynamics. There is no requirement to evaluate or to know the usual structural M, C, K matrices or the aerodynamic loads, and the formulation eliminates the need for a state observer. The controller is firstly implemented numerically and then experimentally on the aeroelastic system. Both frequencies and damping are assigned (together or independently) for the first two vibration modes. The research includes a

---

[*] Research associate, Department Mechanical, Materials and Aerospace Engineering, School of Engineering, Brownlow Hill.

[†] Master Students, Department of Aerospace Engineering, Politecnico di Torino.

[‡] Alexander Elder Professor of Applied Mechanics, Department Mechanical, Materials and Aerospace Engineering, School of Engineering, Brownlow Hill.

[§] Lecturer, Department Mechanical, Materials and Aerospace Engineering, School of Engineering, Brownlow Hill.

procedure for assessing the control effort required and demonstrates an effective means of increasing the flutter margin while the effort is minimized.

Nomenclature

$B, b_j =$ topology input matrix/vector.

$C, C(s) =$ damping matrix, controller transfer matrix.

$c =$ reference wing chord [m].

$d =$ external excitation force [N].

$D_0, D_1, D_2 =$ aerodynamic matrices.

$F, f_j =$ feedback gain matrix/vector.

$f_a =$ aerodynamic force vector.

$f_d =$ disturbance force vector.

$G, g_j =$ feedback gain matrix/vector.

$H(s) =$ receptance matrix.

$H_{am} =$ aerodynamic influence coefficient matrix.

$k =$ reduced frequency.

$K =$ stiffness matrix.

$M =$ mass matrix.

$N =$ number of aerodynamic modes.

$p =$ non-dimensional Laplace variable.

$q =$ dynamic pressure [Pa].

$r(s), r_{\mu_k} =$ transfer matrix, evaluated at $s = \mu_k$.

$s =$ Laplace variable.

$u =$ control force vector.

$v_k, w_k = j^{\text{th}}$ open-/closed-loop eigenvector.

$V =$ air speed [m/s].

$x =$ vector of physical coordinates.

α_j =   arbitrary vector associated with the jth input.

ω_j = j^{th} resonance frequency [rad/sec].

ξ_j = j^{th} modal damping ratio.

$\lambda_j, \mu_j = -\xi\omega_j \pm i\omega_j\sqrt{1 - \xi_j^2}$, j^{th} open-/closed-loop eigenvalue.

σ =   singular value.

I. Introduction

The modification of structural dynamic behaviour, natural frequencies, damping and mode shapes, may be achieved by either passive or active means [1] and, as will be seen later, the problem of aeroelastic flutter suppression may similarly be treated by the so-called 'method of receptances' [2]. We turn first, however, to conventional approaches which stem from a quite separate flow of ideas based on the evaluation of aerodynamic load distributions [3] and their matrix representation [4], as required for state-space aeroelastic control design. Roger, Hodges and Felt [4] extended the uncontrolled flutter velocity of a B52 test aircraft by 10 knots in 1975 by using these techniques. Mukhopadhyay, Newsom and Abel [5] formulated a reduced-order optimal controller for high-order aerodynamic systems. Liebst, Garrard and Adams [6] used eigenstructure assignment (eigenvalues and eigenvectors) in the state-space and a frequency response matching technique. They developed a form of partial pole placement whereby the unstable poles were rotated about the imaginary axis while maintaining the other eigenvalues in the open-loop configuration. Eigenvector shaping was used for gust load alleviation. Andrighettoni and Mantegazza [7] described a cantilevered wing model with leading- and trailing-edge control surfaces and two accelerometers. They developed an ARMAX system-matrix model covering the range of frequencies in which flutter occurs, and eigenstructure assignment was applied robustly to unmodelled disturbances. In the early 2000s a collection of publications [8-10] appeared on research conducted under the Benchmark Active Control Technology (BACT) project at NASA Langley Research Center, where different active aeroelastic control techniques were validated experimentally on a two-degree-of-freedom pitch–plunge transonic airfoil. De Gaspari et al. [11] reported on the development of a built-in wing model with four control surfaces (two leading- and to trailing-edge surfaces) and four accelerometers (two at the wing tip and two at mid-span). A reduced-order model for state-space control implementation was tuned using wind-tunnel results and the resulting controller was found to be capable of damping the wing-bending and torsion modes while

remaining stable within the flight envelope. Bendikson [12] introduced and energy-based approach whereby the system is forced into a stable region of the phase space by altering the aeroelastic mode (bending–torsion amplitude ratio and phase), using minimal control effort. More recently Zhang, Wu and Yang [13] considered the effect of actuator dynamics on the critical flutter velocity, as did Singh, Brown and Kolonay [14] using the method of receptances [2, 15].

The structural-modification theory, from which the receptance method is derived, has been available for many decades [16-18], but only quite recently become practically applicable to physical engineering structures [19-20]. The modern development of 'Transfer Path Analysis' [21], enabling the effects of assembly (or disassembly) of components to be computed using vibration measurements, is based on similar principles. Active modification, using the 'Method of Receptances', was first proposed by Ram and Mottershead [2] for structures equipped with a single control input and several outputs. The method, based on proportional and derivative output feedback, relies only on the measured receptances to determine the controller gains that guarantee the placement of the system poles at the desired locations. The number of complex pole pairs that can be assigned is equal to the number of available sensors. The receptance method has potentially very significant advantages over conventional matrix-based methods such as those described in the first paragraph above. In particular there is no need to know or to evaluate the structural matrices (*M, C, K*) or the aerodynamic coefficient matrices. In addition the use of an observer to estimate unmeasured states is unnecessary because the formulation is in terms of receptance, rather than dynamic stiffnesses. Over the most recent decade the method has been increasingly applied within the research community, leading to several demonstrations, ranging from aeroservoelastic systems [22], flexible structures [23] and vibro-acoustic control [24]. Recently, the receptance method was generalized for Multi-Input Multi-Output systems by the original authors [25] and its efficiency was demonstrated numerically in the active aeroelastic control of a delta wing with multiple trailing edge control surfaces [26]. It was also extended to encompass nonlinear vibration control [27, 28], but until now the MIMO receptance method has not been demonstrated experimentally. The reader who requires further information on research into active flutter suppression in aircraft is referred to [29] for an extensive review.

In this paper, the first experimental validation of the MIMO formulation is demonstrated using a MODular FLEXible aeroelastic wing (MODFLEX) [30], featuring a leading and trailing edge control surfaces and equipped with two position sensors. The paper is organized in five main sections: Section II describes the aeroelastic MODFLEX rig

used for demonstration as well as its numerical model. Section III recalls the formulation of the Multi-Input Multi-Output receptance method and describes its implementation in aeroelasticity. Section IV and V describe, respectively, the numerical and experimental implementation of the receptance method. Finally, the outcomes are summarized in the Conclusions. In addition to the advantages of the receptance method described above, the implementation herein includes the actuator dynamics in the transfer function matrix thereby eliminating the need to model it separately, as in [14].

II. Aeroelastic system

The MIMO receptance based controller is demonstrated numerically and experimentally on the aeroelastic modular flexible wing, referred to as MODFLEX [30]. The aeroelastic model represents a typical finite-length, flexible wing and was designed to exhibit classical flexural-torsional flutter at low airflow velocity. It allows for the implementation of MIMO control strategies.

The dynamics of a structure, described with its mass, damping and stiffness matrices, $M_{n \times n}$, $C_{n \times n}$ and $K_{n \times n}$, is governed by:

$$M\ddot{x} + C\dot{x} + Kx = Bu + f_a + d \tag{1}$$

where $d_{n \times 1}$ represents an external force vector; $u_{m \times 1}$ is a vector of m control input forces, and $B = [b_1 \; b_2 \; ... \; b_m]$ is a $n \times m$ topology matrix, describing the control force distribution over the structure. For aeroelastic systems, f_a represents the vector of generalized aerodynamic forces (GAFs) that can be computed, in the reduced-frequency domain k, by using any numerical method for solving the potential flow.
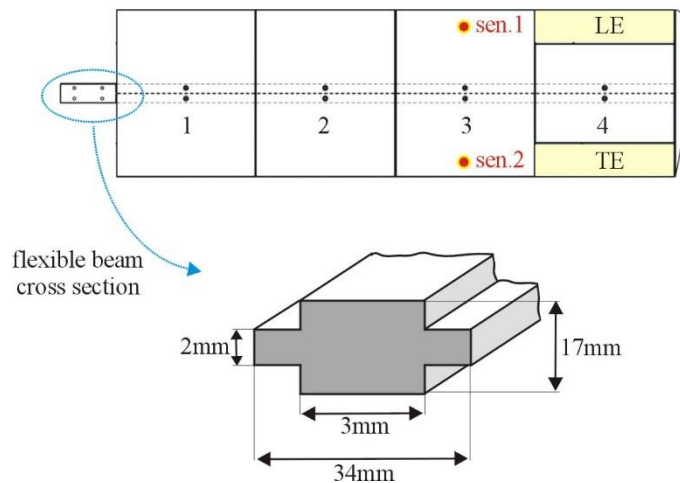
A. Experimental Rig

The MODFLEX wing is made of four sectors, with a NACA0018 profile, mounted on a flexible beam and described in Table 1 and Fig.1. The main spar is made of aluminum alloy and it is the only structural element of the test-rig. By accurately shaping the cross-section of the main spar, the desired flexural, torsional and in-plane stiffness have been achieved (in order to reach a flutter speed well within the 0-20 m/s range of the wind tunnel facility of the University of Liverpool). The main spar is covered by four sectors that provide the correct aerodynamic shape. Each sector is connected to the main spar by two pins at the mid span of the sector so as not to alter the stiffness distribution

of the overall model. The center of gravity and the flexural axis were designed to be coincident on the main spar. The wing model is fully constrained at the built-in end.

The 4th sector is equipped with leading- and trailing-edge aerodynamic control surfaces. Each aerodynamic control surface is actuated with two identical MAXON 60W brushless motors, each with a planetary gearbox and an angular position encoder. Two contactless laser sensors (Keyence LK-500 - mounted on the top of the wind tunnel test section) measure the absolute position of the wing at two distinct points on the 3rd sector, as depicted in Fig.2.

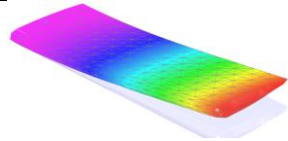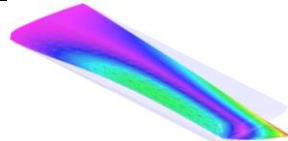| wing data	dimension
wing span	1 m
chord (c)	0.3 m
airfoil	NACA0018
mass axis pos.	0.5×c
flexural axis pos.	0.5×c
motor weight	100 gr

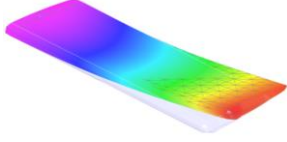**Table 1: MODFLEX main specifications.**

Fig. 1: MODFLEX schematic.
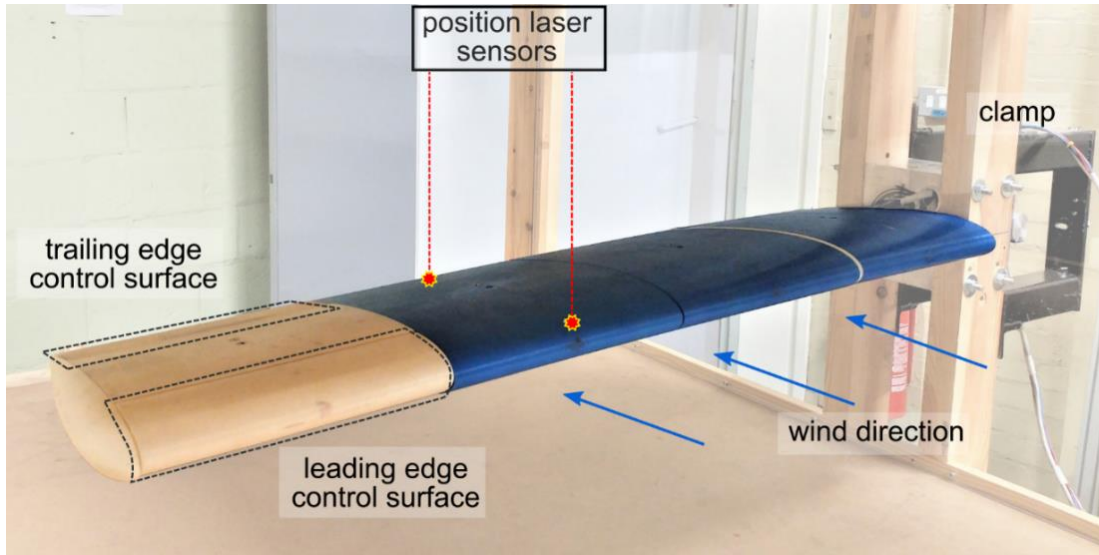
Fig. 2: MODFLEX experimental setup.

B. Finite element model

A finite-element model coupled with unsteady aerodynamics was produced to assist in the design of the MODFLEX aeroelastic wing. Of course, the model has no direct role in the design of the controller, which is based entirely on measured receptances (or transfer functions). The model consists of a beam-element model with distributed lumped masses to count for the mass distribution of the sectors and the servomotors used for driving the control surfaces (developed in MD.Nastran). Aerodynamic panels are added to the finite element model to solve the potential flow via the Doublet Lattice Method (DLM). Structural modal damping of 2% was assumed.

Mode	ω_i [Hz]		ξ_i [%]		Mode shape
	Num.	*Exp.*	*Num.*	*Exp.*	
first bending - 1B	2.97	2.84	6.7	7.0	
first torsion - 1T	4.41	4.11	4.9	3.4	

first in-plane - 1P	6.97	6.41	1.14	-	

Table 2: Modal data of the flexible wing: wind speed $V = 10\text{m/s}$.

A preliminary modal analysis campaign was conducted for checking the behavior of the experimental model against the numerical one. In Table 2 the numerical data, in terms of frequency ω_i and damping ξ_i, are compared with the experimental data for an airspeed of $V =$10m/s; only the first two modes are relevant for the flutter mechanism investigated. More detail on the comparison between the experimental and the numerical model can be found in Appendix A.

C. Flutter test

A flutter test comparison was performed with the velocity vs. frequency and velocity vs. damping diagrams, by computing frequency and damping of the 1st bending and the 1st torsional modes at different air speeds. For the experimental wing, the frequency and the damping values were obtained by a combination of impact-hammer and stepped-sine excitations (by the aerodynamic surfaces), at airspeeds that were increased incrementally until close to the flutter velocity. The numerical data were computed by solving the *p-k* continuation method within MD.Nastran SOL145.

Figure 3 compares the numerical and the experimental results. Numerically, it results a flutter velocity of 16m/s, while experimentally the flutter instability occurs at a wind speed of 13.5m/s. The lower flutter speed for the experimental model is in agreement with the smaller (negative) values of damping shown in Fig.3.b. As stated previously, the main purpose of the numerical model is to assist in the design of the aeroelastic wing. It does have another use in demonstrating the working of the receptance method (Section IV). The experimental results, in terms of natural frequencies, modes and flutter velocity, confirm that the performance of experimental rig is entirely within the capability of the Liverpool low-speed wind tunnel. Since the controller is based on experimental measurements, ant not on the numerical model, it is unnecessary to tune the model to fit the data. In what follows, the control system will be targeted on the first bending (1B) and the first torsional (1T) modes.

D. Dynamic model

A state space (SS) model of MODFLEX is developed for preliminary numerical validation of the receptance-based controller. The structural and aerodynamics matrices are extracted and rearranged in the style of Eq.(1) where $f_a = qH_{am}(k, M)x$ and H_{am} is the aerodynamic influence coefficient matrix. The state space model is arranged in such a way that the inputs are the torques applied at the hinges of the control surfaces, and the outputs are the angular positions of the control surfaces and the absolute vertical position of the two degrees of freedom located at the 3rd sector.
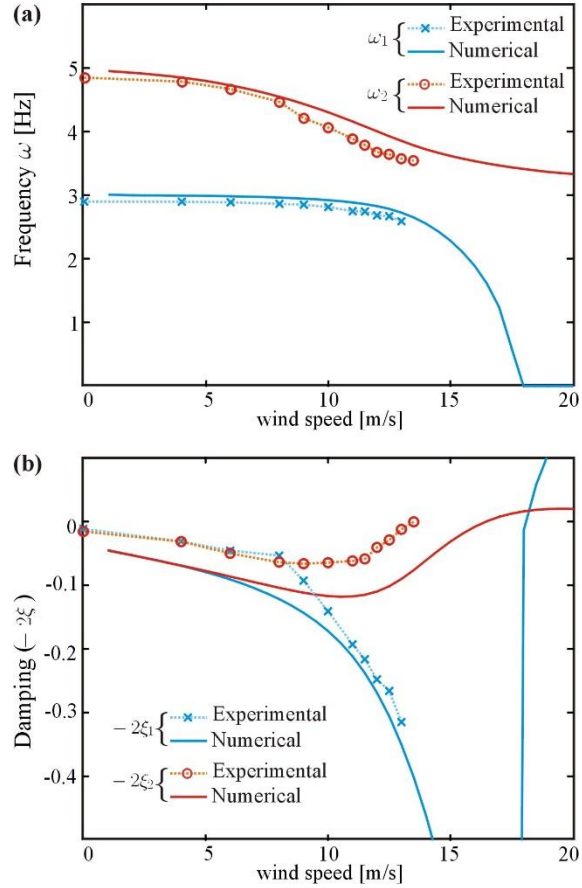
Figure 3: Numerical vs. experimental velocity vs. frequency and velocity vs. damping (-2ξ) diagrams of the MODFLEX wing.

The model is reduced to include only the states associated with the first bending, torsional and in-plane flexible modes (1B, 1T and 1P in Table 2), four states associated with the two rigid body modes of the control surfaces and five aerodynamic states. The aerodynamic states are obtained by fitting the matrix of aerodynamic influence coefficients, H_{am}, using the Roger's classical expansion [3],

$$f_a = q\left(D_0 + D_1 p + D_2 p^2 + \sum_{i=1}^{N} \frac{p}{p - \beta_i} E_i\right) x \tag{2}$$

where

$$p = \frac{c}{2V} s \tag{3}$$

is the non-dimensional Laplace variable; q is the dynamic pressure of the flow. The terms D_0, D_1 and D_2 are aerodynamic matrices contributing to the stiffness, damping and mass matrices, respectively. The fourth term accounts for the fluid-structure coupling, such that N is the number of modes and β_i and E_i are respectively, arbitrary values in the frequency range of interest, and matrices of real least-squares coefficients. The dynamics of the aeroelastic system is then obtained by substituting Eq.(2) into Eq.(1), leading to

$$\left[M - q\left(\frac{c}{2V_\infty}\right)^2 D_2\right] \ddot{x} + \left[C - q\frac{c}{2V_\infty}\left(D_1 + \sum_{i=1}^{N} \frac{1}{p - \beta_i} E_i\right)\right] \dot{x} + [K - qD_0]x = Bu \tag{4}$$

with the system expressed in physical coordinates, Eq.(4) is very similar to Eq.(1), but with additional wind-speed-dependent mass and stiffness matrices, and wind-speed- and a frequency-dependent damping matrix. In this configuration, the matrix B expresses the distribution of the input torques at the hinges of the control surfaces. Thus, without any loss of generality, the same formulation of the receptance method, recalled for flexible structures in the following, applies also to aeroelastic systems.

E. Low Authority Control of the aerodynamic surfaces

The controller of the aeroelastic wing, illustrated in Fig.4, is built in two cascaded control loops: *(i)* a low authority control loop (LAC) which controls the angular position of the aerodynamic control surfaces, and *(ii)* a high authority control loop (HAC) where any active aeroelastic controler can be implemented; in this case, the receptance-based controller for partial pole placement as described in Section III. The purpose of the LAC is to dynamically control the position of the control surfaces in order to generate the desired torque at the hinges of the control surfaces. In addition, it stabilizes the leading edge flap. The PID controllers were tuned at zero airspeed and have a bandwidth of 30 Hz for the trailing edge and more than 100 Hz for the leading edge, their dynamics is well above the aeroelastic modes of interest. It should be noted that $d = (d_1, d_2)^T$ in Fig.4(a) represents a disturbance input. Due to the rigid body dynamics of the leading edge control surface (facing the wind flow), the model is inherently unstable. Furthermore, the aeroelastic control is more convenient if the position of the control surfaces is directly commanded instead of the

10

torque. Therefore, in order to stabilize the system and use the position of the aerodynamic control surfaces as a command, a low authority control loop (LAC) is implemented for each control surface. A Proportional-Integral-Derivative (PID) controller uses the angular position of the control surface (measured with a position encoder) to calculate the appropriate torque to apply in order to maintain the control surface at a desired position (internal loop in Fig.4.a). The control bandwidth of the PID controllers is relatively high, with respect to the dynamics of the flexible wing, and it was checked experimentally up to 15Hz; for both loops, it is estimated to be higher than 30Hz. With such a configuration, the input of the system becomes the control surface angular position $u = (u_{LE}, u_{TE})^T$, and the outputs remain the absolute positions measured at two different points of the flexible wing $y_x = (x_1, x_2)^T$.
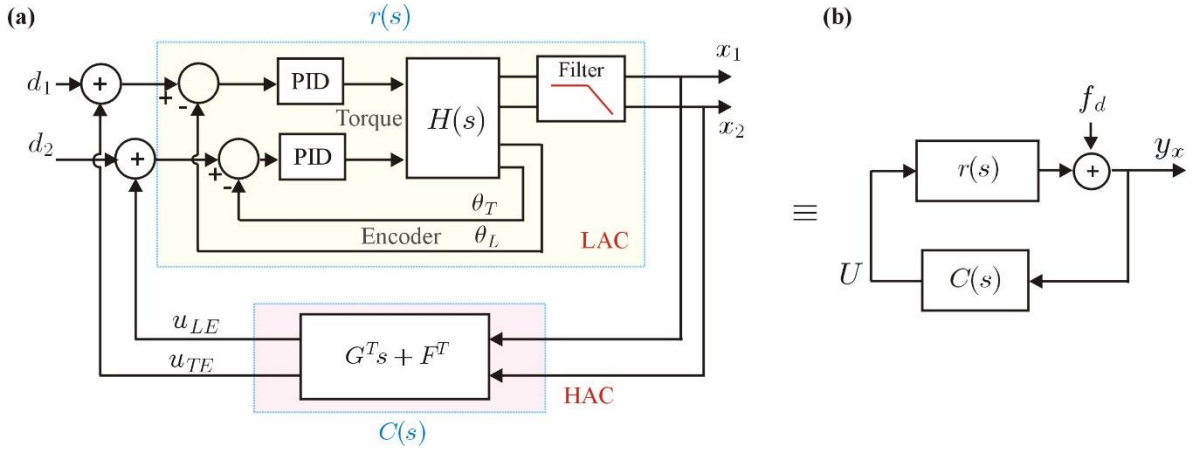
Figure 4: Bloc diagram of the HAC-LAC control architecture. (a) Detailed bloc-diagram; (b) equivalent bloc diagram, with $f_d = R(s)(d_1, d_2)^T$. The receptance-based controller, presented in the following section, is

$$C(s) = F^T s + G^T.$$

III.Pole placement with the receptance method

In this section, the Multi-Input Multi-Output (MIMO) receptance method is recalled. The original theory [25] was given in terms of the receptance transfer function, but is in fact applicable to transfer functions of any form. In the present case, the theory presented in terms of the matrix of transfer functions $R(s)$ relating the encoder control surface positions $(u_{LE}, u_{TE})^T$ as inputs to the output laser displacements measurements $(x_1, x_2)^T$ at two locations on the wing, as shown in Fig. 2. The receptance method proposes a systematic control design procedure for pole placement, without any use of state observers or underlying numerical models. The number of pole pairs which can be placed is equal to

the number of sensors. Thus for the control of the aeroelastic wing, with 2 sensors, we aim to modify the eigenpairs associated with the two first modes.

Consider the system of Eq.(4), where the matrices $\tilde{M}$, $\tilde{C}$ and $\tilde{K}$ are inclusive of the aerodynamic terms. The matrix $H(s)$ in Fig. 4 is then given by $\left(\tilde{M}s^2 + \tilde{C}s + \tilde{K}\right)^{-1}$. The input-output transfer function in question is not $H(s)$ but $R(s)$, where

$$y_x = R(s)u \tag{5}$$

Assuming a proportional and derivative feedback control, i.e.

$$u = F^T\dot{x} + G^Tx, \tag{6}$$

The receptance method offers a straightforward procedure aimed at determining the feedback gains F and G by using only the measured transfer function $R(s)$.

A. The method

The theory will be presented here for the general case of a system with 2n poles, although specifically $n = 2$ in the present example. Therefore, let μ_k, $k = 1, 2, \dots, p$, be the set of desired poles to be assigned, distinct from the open-loop poles λ_k, $k = 1, 2, \dots, 2n$, such that the poles for $k = p + 1, p + 2 \dots, 2n$ remain unchanged; and let $r(s) = R(s)B$ be the measured transfer-function matrix between the control inputs and outputs, where B denotes the force distribution matrix (in the present example $B = \begin{bmatrix} 1 & 0 \\ 0 & 1 \end{bmatrix}$). The control feedback gains $F = [f_1\ f_2 \dots f_m]$ and $G = [g_1\ g_2 \dots g_m]$ can be found by solving the linear equation:

$$\begin{pmatrix} P_1 \\ P_2 \\ \vdots \\ P_p \\ Q_{p+1} \\ Q_{p+2} \\ \vdots \\ Q_{2n} \end{pmatrix} \begin{bmatrix} f_1 \\ \vdots \\ f_m \\ g_1 \\ \vdots \\ g_m \end{bmatrix} = \begin{bmatrix} \alpha_1 \\ \alpha_2 \\ \vdots \\ \alpha_p \\ 0 \\ 0 \\ \vdots \\ 0 \end{bmatrix} \tag{7}$$

where

$$P_k = \begin{bmatrix} \mu_k w_k^T & 0 & \dots & 0 & w_k^T & 0 & \dots & 0 \\ 0 & \mu_k w_k^T & \dots & 0 & 0 & w_k^T & \dots & 0 \\ \vdots & \vdots & \ddots & \vdots & \vdots & \vdots & \ddots & \vdots \\ 0 & 0 & \dots & \mu_k w_k^T & 0 & 0 & \dots & w_k^T \end{bmatrix}, \tag{8}$$

$$Q_k = \begin{bmatrix} \lambda_k v_k^T & 0 & \cdots & 0 & v_k^T & 0 & \cdots & 0 \\ 0 & \lambda_k v_k^T & \cdots & 0 & 0 & v_k^T & \cdots & 0 \\ \vdots & \vdots & \ddots & \vdots & \vdots & \vdots & \ddots & \vdots \\ 0 & 0 & \cdots & \lambda_k v_k^T & 0 & 0 & \cdots & v_k^T \end{bmatrix}, \tag{9}$$

$$\alpha_k = \begin{bmatrix} \alpha_{\mu_k,1} & \alpha_{\mu_k,2} & \cdots & \alpha_{\mu_k,m} \end{bmatrix}^T \in \mathbb{C}^{m \times 1} \tag{10}$$

and

$$w_k = \alpha_{\mu_k,1} r_{\mu_k,1} + \alpha_{\mu_k,2} r_{\mu_k,2} + \cdots + \alpha_{\mu_k,m} r_{\mu_k,m}, \tag{11}$$

where $r_{\mu_k,j}$ stands for the jth column of $r(\mu_k) = R(\mu_k)B$, or alternatively $r_{\mu_k,j} = R(\mu_k)b_j$, and v_k denotes the retained eigenvectors, which are computed directly from the measured open-loop transfer-function matrix, while w_k are the eigenvectors of the closed-loop system, where

$$w_k = r(\mu_k)(F^T \mu_k + G^T)w_k. \tag{12}$$

The w_k terms are chosen a priori, by a careful choice of the weighting parameters $\alpha_{\mu_k,j}$, $(j = 1, \dots, m)$. Indeed, the parameters $\alpha_{\mu_k,j}$ determine the participation of the jth control input for the assignment of the kth mode. Each choice of appropriate parameters $\alpha_{\mu_k,j}$ results in a new set of feedback gains F and G. In [11] they are chosen in such a way that the eigenvectors of the controlled system w_k remain identical to the eigenvectors of the uncontrolled system v_k; in this study, by exploring numerically all the possible combinations, we choose such parameters $\alpha_{\mu_k,j}$ in order to minimize the control effort.

Finally, once the parameters $\alpha_{\mu_k,j}$ are found, the closed-loop eigenvectors w_k are constructed and the matrices P_k and Q_k are easily built. The feedback gains F and G are then found by following the five steps in the flowchart of Fig.5.
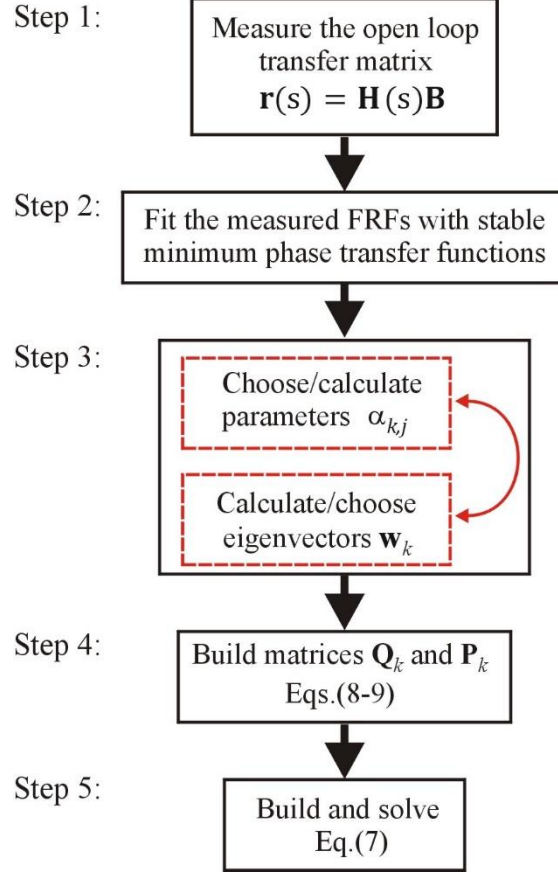
Figure 5: Flowchart: Calculation of feedback gains by the receptance method.

Remark: In theory, the parameters $\alpha_{\mu_k,j}$ can be chosen arbitrarily; however, this may lead to a high control effort for some actuators and a smaller one for the others. From Eq.(7-10), it is clear that $\alpha_{\mu_k,j}$ are weighting factors on the jth control input; if $\alpha_{\mu_k,j} = 0$, then the jth actuator will not contribute to the control of the kth pole; inversely, if $\alpha_{\mu_k,j} \gg \alpha_{\mu_k,i} \ (i \neq j)$, then the kth pole will be mainly controlled with the jth actuator. Alternatively, if the parameters $\alpha_{\mu_k,j}$ are all equal, then the feedback gains of each input j, f_j and g_j, will be identical for all the control loops. An obvious way to tune $\alpha_{\mu_k,j}$ is to choose them proportionally to the control input authority over the assigned mode (e.g. proportional to the modal amplitudes at the input location). The selection of the parameters $\alpha_{\mu_k,j}$ in an optimal way (e.g. minimizing the overall control effort) remains an open problem and will not be addressed in this study. Nevertheless, when the measurement of all the degrees of freedom of the structure is available, it can be shown that the vector α_{μ_k} that corresponds to the minimum control effort is obtained by choosing the closed-loop eigenvector w_k equal to the open-loop eigenvector v_k.

14

B. Aeroelastic implementation of the receptance-based controller

The receptance-based controller is implemented as depicted in the block diagram of Fig.4. The open-loop transfer-function matrix $R(s)$, relating the control inputs $u = (u_{LE}, u_{TE})^T$ (the angular position of the control surfaces) to the position of the wing $y_x = (x_1, x_2)^T$, is used to calculate the feedback gains F and G, by following the procedure described previously.
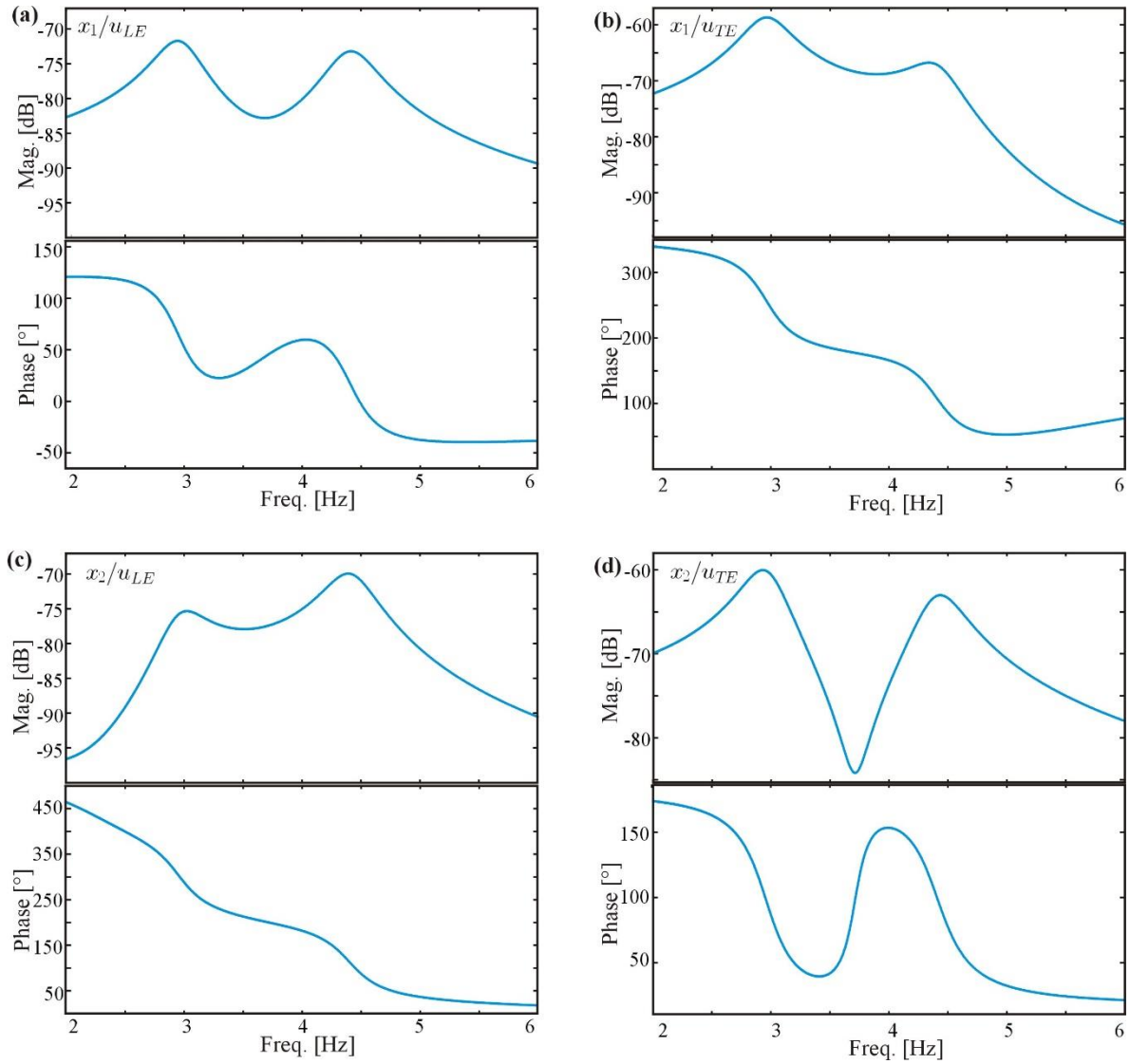
Figure 6: Numerical model: Open-loop frequency response functions $r(s)$ at wind speed $V = 10$m/s. (a) x_1/u_{LE}; (b) x_1/u_{TE}; (c) x_2/u_{LE}; and (d) x_2/u_{TE}.

15

The numerical and the experimental implementation of the receptance-based controller is carried out exactly in the same manner, as shown in the architecture of Fig.4. First, the LAC loop implementing the PID controller is used to drive the angular position of the control surfaces; with the LAC controllers engaged, the open-loop transfer-function matrix of the system $r(s)$ is measured at a wind speed 10m/s. Fig.6 shows the FRFs of this $r(s)$ for the numerical system.
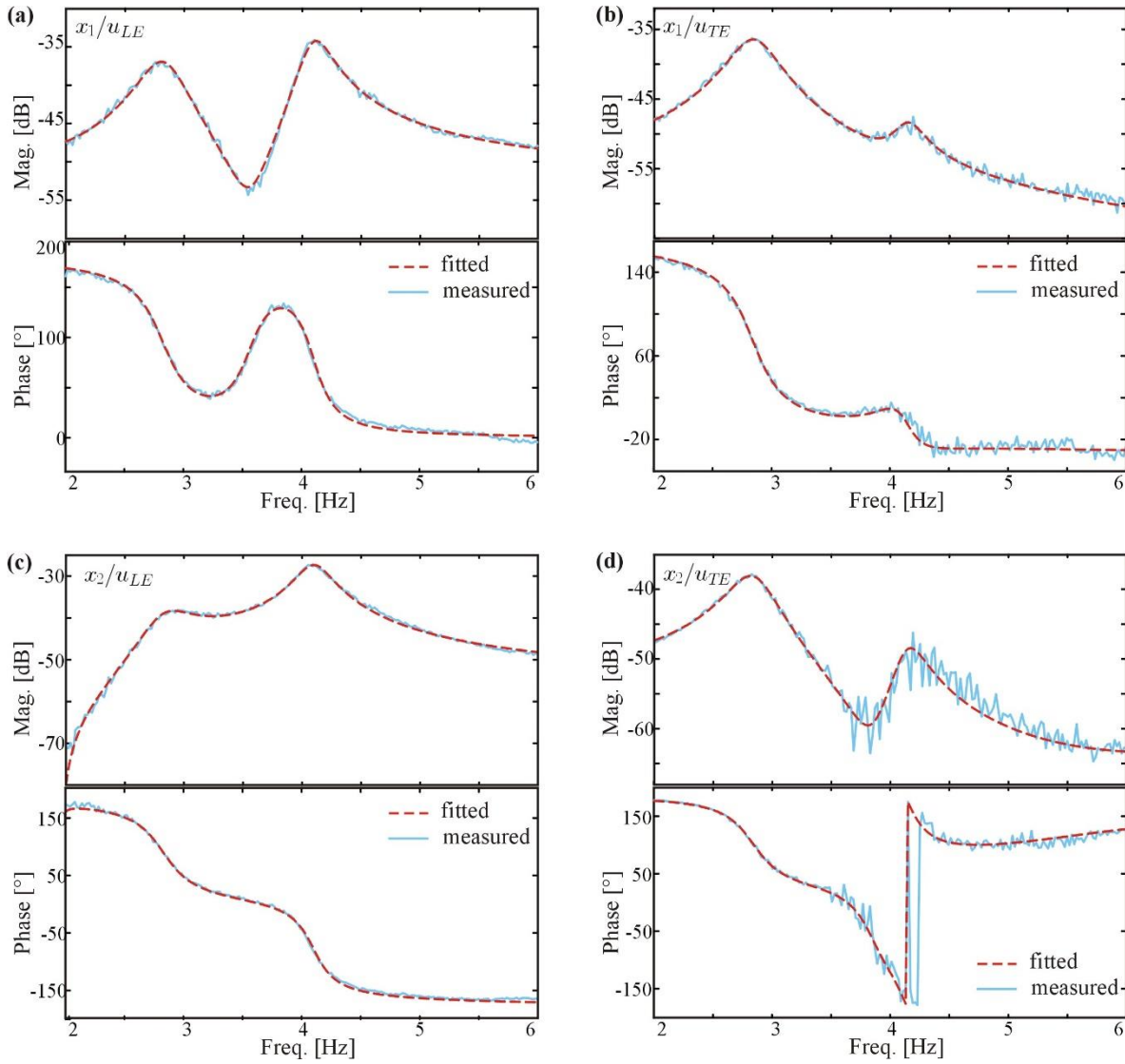
Figure 7: Measured vs. fitted open-loop frequency response functions $r(s)$ at wind speed $V = 10$ m/s. Inputs: angular positions of the control surfaces (u_{LE}, u_{TE}). Outputs: position of the flexible wing (x_1, x_2).

In the experimental case, an additional step is necessary: the measured input-output FRFs, Fig.7, are fitted with stable minimum-phase transfer functions, using SDTools toolbox, while the modal data are identified using the

PolyMAX technique [28]. The open-loop transfer functions of the system are measured by exciting the control surfaces with a stepped sine oscillation (u_{TE} and u_{LE} in Fig.4), over the frequency range of interest, 2 to 6Hz. A single control surface is excited at a time.

Once the open-loop transfer-function matrix of the system $R(s)$ is obtained, the receptance- based pole placement controller is implemented exactly as described in the previous section. The control is targeted for the first two modes, 1B and 1T and ignores the higher frequency modes. A second order Butterworth filter, with a cross-over frequency at 10Hz, has been placed in series with the controller; it is necessary for the stability of the system, as it limits the control bandwidth and adds a roll off at high frequencies to avoid spill-over. As discussed previously, the parameters $\alpha_{\mu_k,j}$ are selected to minimise the control effort, by exploring numerically all the possibilities.

IV.Numerical Results

Several control scenarios are considered, where the modal resonant frequencies and damping coefficients are alternatively or simultaneously modified. Control scenarios different from the experimental implementation (in Section IV) are chosen. Fig.8 shows the frequency response function of the controlled system (x_1/d_1) when the first mode is targeted while the second mode is kept unchanged; the figure shows the response when: (a) the damping ratio of the first mode is doubled (red dashed curve) or tripled (blue solid curve), and (b) when only the resonant frequency is increased (blue solid curve) or decreased (red dashed curve) by 20%. Fig.9 shows the same FRF when the two modes are modified simultaneously, such that: (a) the damping of both modes is doubled; or (b) the spacing between their resonance frequencies is increased by $\pm20\%$. For each control scenario, the poles are placed exactly at the desired positions.
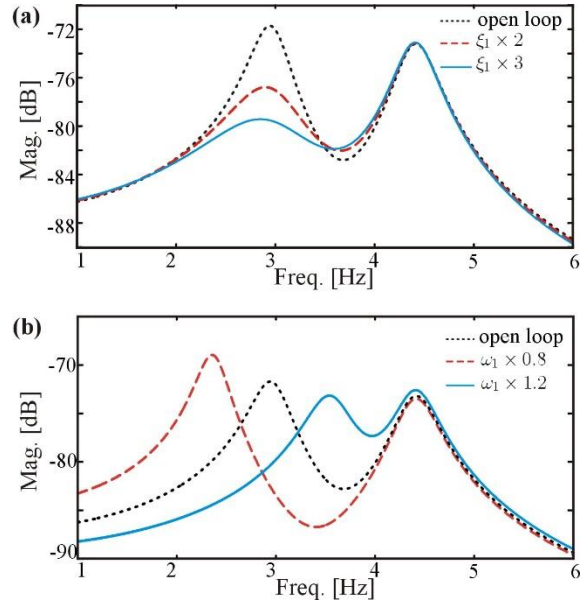
Figure 8: FRF of x_1/d_1: mode 1B is targeted. (a) open-loop ($\cdots$ dotted line), $\xi_1 \times 2$ (--- red dashed line)

and $\xi_1 \times 3$ ($-$ blue solid line). (b) open-loop ($\cdots$ dotted line), $\omega_1 \times 0.8$ (--- red dashed line)

and $\omega_1 \times 1.2$ ($-$ blue solid line).
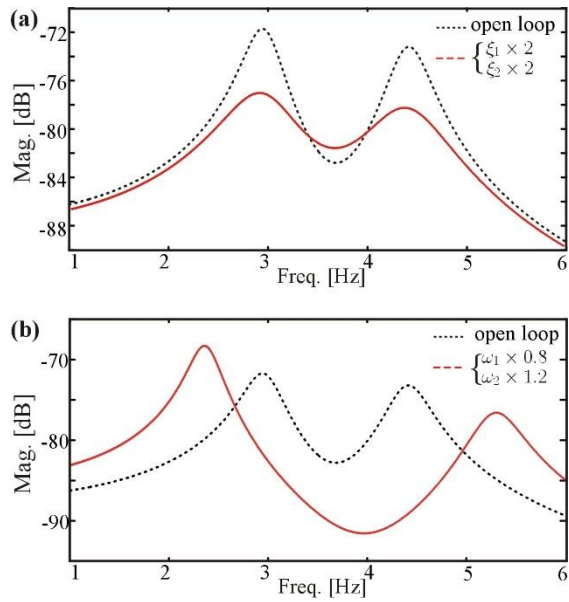
Figure 9: FRF of x_1/d_1: open-loop ($\cdots$ dotted line) and closed-loop ($-$ red solid line). (a) $\xi_1 \times 2$ and $\xi_2 \times 2$.

(b) $\omega_1 \times 0.8$ and $\omega_1 \times 1.2$.

Control effort - selection of α_{μ_k}

For each control scenario presented previously, the poles of the closed-loop system have been placed exactly at the desired location, despite the choice of the parameter α_{μ_k}. However, for each combination of the parameters α_{μ_k}, the arising control gains F and G are different, and may be infinite under certain conditions (when Eq.(7) becomes singular). As described in Appendix B, the control effort can be assessed by simply evaluating the singular values of the transfer-function matrix relating the disturbance vector $f_d = r(s)(d_1, d_2)^T$ to the control commands $u = (u_{TE}, u_{TE})^T$. From Fig.4, it can be shown that:

$$u = C(s)[I - R(s)C(s)]^{-1} f_d = G_d(s)f_d \tag{13}$$

Where $C(s) = F^T s + G^T$ is the receptance-based controller, and $R(s)$ is the transfer-function matrix, relating the control inputs to the outputs.
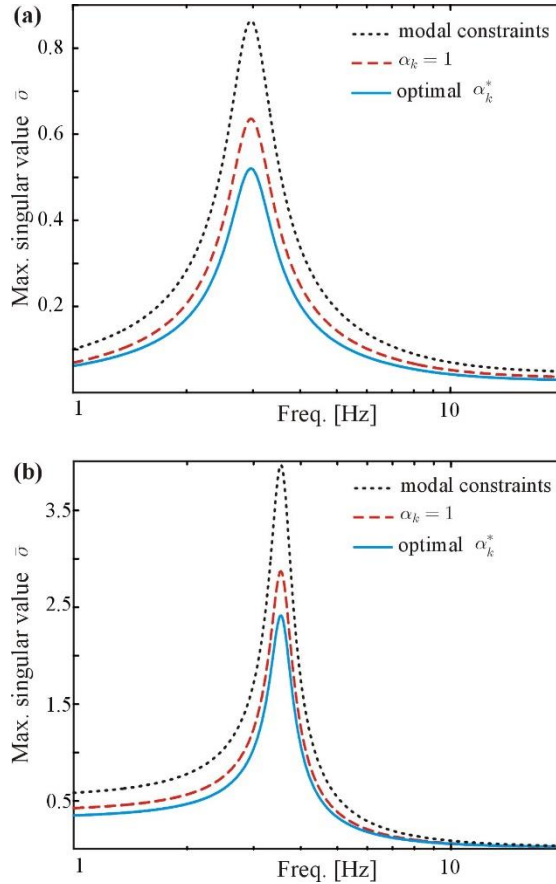
Figure 10: Maximum singular value $\bar{\sigma}$ of $G_d(s)$ with various choice of the parameters α_k. The control is targeted for increasing (a) $\xi_1 \times 2$; and (b) $\omega_1 \times 1.2$.

Figure 10 compares the maximum singular values $\bar{\sigma}$ of the transfer-function matrix $G_d(s)$ for three different choices of the parameters α_{μ_k}: *(i)* when the parameters are chosen to conserve the mode shape of the targeted mode, *(ii)* when they are chosen to minimize the control effort, and *(iii)* when they are chosen all equal to 1 (i.e. all the actuators have the same feedback gains and react with the same amplitude). The control is targeted either for increasing the damping of the first bending mode (Fig.10.a), or for reducing the resonance frequency by 20%, Fig.10.b. For both cases, the control effort is not necessarily the smallest when the parameters α_{μ_k} are chosen to preserve the mode shapes and it may lead to infeasible controllers (due to the stroke of the actuators). In this example, the optimal value of α_{μ_k} which minimizes the control effort has been found by exploring the whole space. Further investigations to determine analytically the optimal α_{μ_k} will be conducted in a separate study.

V. Experimental Results

Several control scenarios are implemented in the experimental campaign, and they are summarized in Table 3. Tests #1 to #3 are targeted for increasing the damping of the first bending (1B) and the first torsional (1T) modes, while tests #4 and #5 are targeted for modifying their resonance frequencies; the associated FRFs x_1/d_1 with and without control are shown in Fig.11 and Fig.12, respectively. Clearly in all of the tests the imaginary part is an order of magnitude greater than the real part. For the three first tests, the error on the pole location is negligible, and it is mainly associated with the smaller real part of the pole (i.e. the damping component of the pole).

	Test	Desired pole location		New pole location	
		$\mu_{1,2}$	$\mu_{3,4}$	$\mu_{1,2}$	$\mu_{3,4}$
#1	$\xi_{1T} \times 2$	$-1.25 \pm 17.8j$	$-1.76 \pm 25.8j$	$-1.42 \pm 17.8j$	$-1.78 \pm 25.3j$
#2	$\xi_{1T} \times 3$	$-1.25 \pm 17.8j$	$-2.63 \pm 25.7j$	$-1.41 \pm 17.7j$	$-2.7 \pm 25.5j$
#3	$\xi_{1B} \times 2$ and $\xi_{1T} \times 2$	$-2.5 \pm 17.7j$	$-1.76 \pm 25.8j$	$-2.33 \pm 17.7j$	$-1.72 \pm 25.1j$
#4	$\omega_{1T} \times 1.2$	$-1.25 \pm 17.8j$	$-1.05 \pm 31j$	-1.67 ± 17.8	$-1.8 \pm 31.3j$
#5	$\omega_{1B} \times 0.9$ and $\omega_{1T} \times 1.1$	$-1.13 \pm 16j$	$-0.97 \pm 28.4j$	$-1.26 \pm 16j$	$-1.36 \pm 28.2j$

Table 3: Closed-loop control test campaign conducted on the flexible wind. New pole location vs. desired pole location.

Similarly, for test #4 and #5, one can consider the error on the new pole locations to be negligible for the imaginary part of the pole (and the resonance frequency). However, especially for these two tests, the error in the damping is relatively high and may reach 66% (in test #4, $\xi_{1T} = 5.7\%$ instead of 3.4%); this may be associated to the fact that the control surface deflection is very high, which possibly results in additional aerodynamic damping.
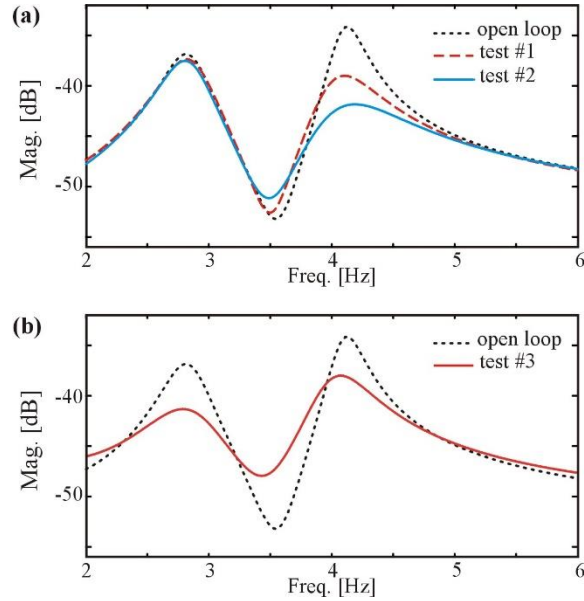

Figure 11: Measured FRF x_1/d_1 with and without control (dotted line $\cdots$): tests (a) #1 (dashed line ---) and #2 (solid line $-$); (b) #3 (solid line $-$).
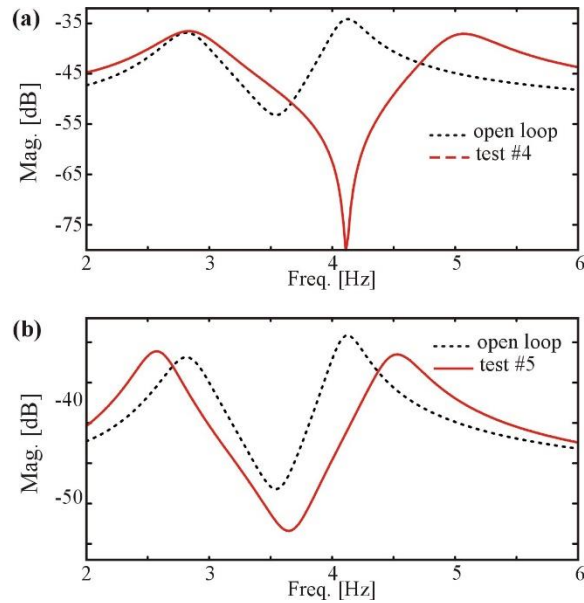
Figure 12: Measured FRF x_1/d_1 with (solid line $-$) and without control (dotted line $\cdots$): test (a) #4; (b) #5.

A. Control effort

The control effort of the system has been measured by calculating the singular values of the transfer-function matrix relating the input vector $f_d = R(s)(d_1, d_2)^T$ and the computed commands $(u_{LE}, u_{TE})^T$, as mentioned earlier and described in Appendix B. Fig.13.a shows the maximum singular values $\bar{\sigma}$ associated with the tests #1, #2 and #3, where the control is targeted only for the damping. When only the second mode 1T is targeted, the control effort reaches a maximum around this mode, while there is no peak around the first mode; this is due to the nature of the receptance based control which works in a similar way to a modal filter, as expressed by the constraint $Q_k[f_k^T \quad g_k^T]^T = 0$ in Eq.(7).
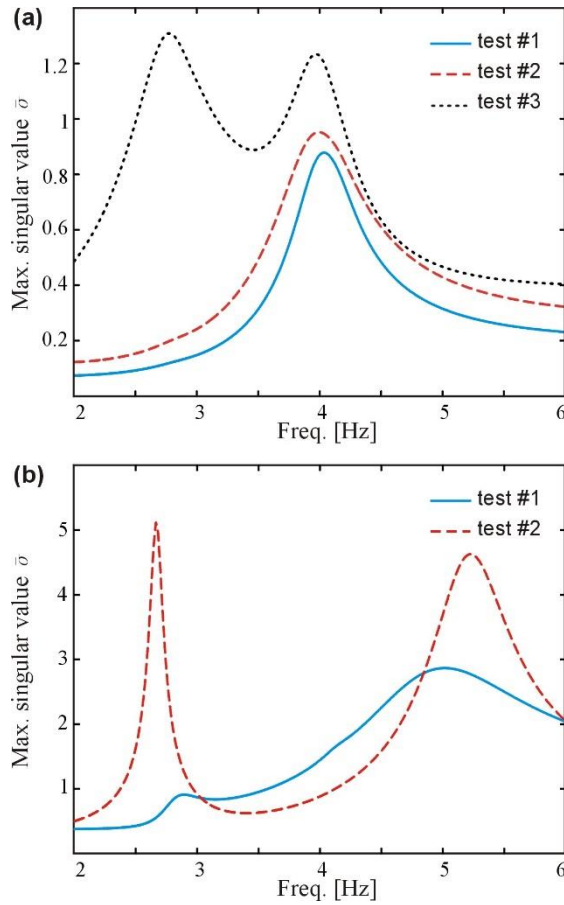
Figure 13: Control effort: measured $\bar{\sigma}$ of the transfer-function matrix between $(d_1, d_2)^T$ and the computed commands $(u_{LE}, u_{TE})^T$: (a) tests #1, #2 and #3 ; and (b) test #4 and #5.

Figure 13.b shows $\bar{\sigma}$ for tests #4 and #5, where the control is targeted for shifting the resonance frequencies of the modes of interest, 1B and 1T. The control effort is significantly higher, compared to the tests when only the damping is increased, and was at the limit of the control surfaces stroke (with relatively small disturbances). This fact could be also observed from the calculated gains that are one order of magnitude higher in test #4 and #5 than in test #1, #2 and #3. Once again, when only a single mode is targeted, the control effort is concentrated around this mode. Recall that for the various control tests conducted on the aeroelastic wing, the parameters α_{μ_k} have been chosen in order to minimize the control effort, and thus, without a careful choice of α_{μ_k}, the controller would not be feasible.
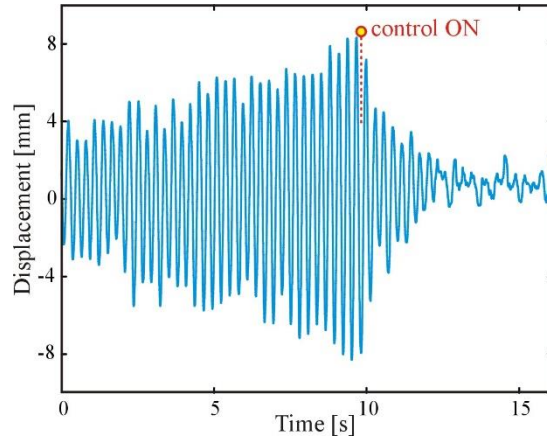
B. Flutter control

A flutter test was carried out for the five active control tests depicted in Table 4. The wing is positioned in the wind tunnel, with the control surfaces positioned at zero angular position (aligned with the wing), while the control is turned on. The wind speed is then increased progressively until the flutter speed is reached. Table 4 depicts the flutter speed for each control test; test#0 is the reference case, in which only the LAC loop is active, and the system exhibits a flutter speed of 13.5m/s.

The experimental campaign showed that increasing the damping of the torsional mode (test #2) is the most efficient way to increase the flutter speed, as the flutter occurs when the damping of this mode becomes negative. Fig.14 shows the time response of the position sensors x_1, near an air speed of 13.5m/s, without HAC control and when the control is turned near the 10th s; the control corresponds to test #2 where the damping of the torsional mode is tripled.

|	Test	Flutter speed [m/s]
#0	Open-loop	13.5
#1	$\xi_{1T} \times 2$	15.5
#2	$\boldsymbol{\xi_{1T} \times 3}$	**16.5**
#3	$\xi_{1B} \times 2$ and $\xi_{1T} \times 2$	15.5
#4	$\omega_{1T} \times 1.2$	14
#5	$\omega_{1B} \times 0.9$ and $\omega_{1T} \times 1.1$	15

Table 4: Flutter speed with various control configurations.

Figure 14: Measured wing position during flutter at wind speed 13.5m/s. The control is turned ON near the 10th second. The control is tuned to triple the damping of the torsional mode 1T (test #2).

The experimental velocity vs. frequency/damping (where the damping is expressed as -2ξ) diagrams are plotted in Fig.15, with and without control. The control is tuned to triple the damping of the torsional mode 1T (test #2). As imposed by the control design, only the damping of the 1st torsional mode is increased, while the resonance frequencies of the 1B and 1T modes remain almost identical to the open-loop system. It is clearly seen that the control shifts down the damping curve of the torsional mode, responsible of flutter. Notice also that, even at rest, without any flow around the wing, i.e. $V = 0$m/s, the control still provides significant damping to the targeted mode; this is possible due to the relatively high inertia of the leading-edge control surface which causes it be behave like an inertial actuator.
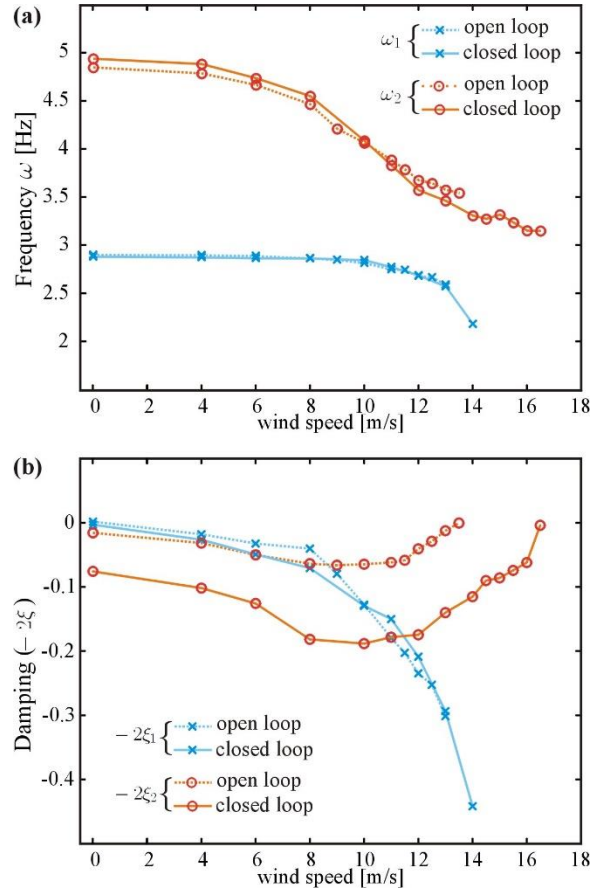
Figure 15: Measured (a) frequency (ω), and (b) damping (-2ξ) as a function of the wind speed. Open-loop (--- dashed line) and closed-loop (− solid line). The control is tuned to triple the damping of the torsional mode 1T (test #2).

Finally, one should note that the controller has been tuned based on a model at wind speed 10m/s, and has not been adapted as the wind speed evolves. Although the control proves to be effective, it would be worthwhile for the feedback gains to be adapted as a function of the wind speed.

VI.Conclusions

In this paper, a pole-placement controller, designed by using the Multi-Input Multi-Output receptance method, was implemented both numerically and experimentally for the first time on an aeroelastic system. The method considers proportional and derivative position feedback and relies only on the measured input-output frequency response functions to calculate the controller gains. The efficiency and accuracy of the method is demonstrated through

a set of control scenarios applied on an aeroelastic wing where the receptance-based aeroelastic control proved capable of assigning both frequencies and damping, both individually and together.

Following the test campaign and the numerical simulations, the following main concluding remarks may be made:

(i)   The study demonstrates the merits of the receptance method in simplifying the control design for active vibration control of flexible structures in general, without any need for a quantitative numerical model or the use of state observers.

(ii)   The method applied in the study eliminates the need to model the actuator dynamics separately; it is included in the measured input-output transfer function.

(iii)   A numerical search procedure based on singular value decomposition of the transfer-function matrix between the disturbance vector $f_d = r(s)(d_1, d_2)^T$ and the control commands $u = (u_{TE}, u_{TE})^T$ may be used to determine the minimum control effort.

(iv)   The parameters $\alpha_{\mu_k}, k = 1, 2, \cdots, m$ define the kth closed-loop mode shape. Selecting α_{μ_k} such that the closed-loop and open-loop modes are identical (at the output degrees of freedom) does not in general lead to the lowest control effort.

(v)   A low pass filter may be used as a practical solution to avoid the spill-over of high-frequency modes when the number of sensors is limited. This may lead to increased control effort and could be difficult to apply in the case of close modes.

(vi)   An increase in the flutter velocity of around 22% was achieved for the modular flexible wing that formed the object of the test.

VII. Appendices

A. Appendix A – MODFLEX

Structural characterization of the MODFLEX numerical/experimental system in terms of frequency, damping and mode shape are depicted in Table 5 and Fig.16.
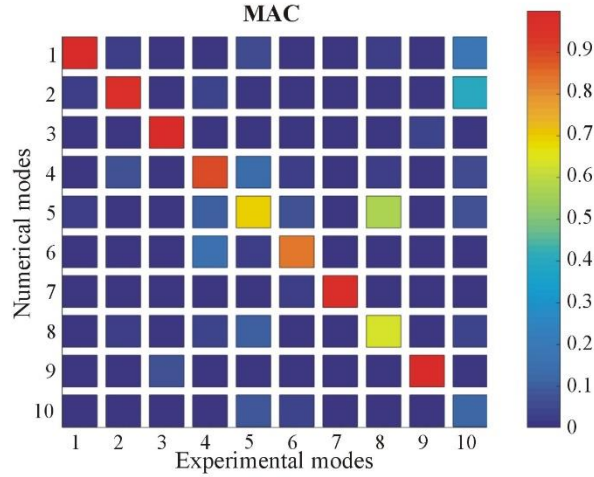
Figure 16: Modal Assurance Criterion (MAC) for the first 10 mode shapes obtained by the numerical and the experimental model, $V = 10\text{m/s}$.

Mode	Mode shape	Numerical model Freq. [Hz]	Experimental model Freq. [Hz]	Damp ξ [%]	Error %
1	1st bending	3.03	2.9	0.24	4.5
2	1st torsional	4.97	4.81	0.65	3.3
3	1st in-plan	6.97	6.41	1.14	8.7
4	2nd torsional	15.07	14.64	1.22	2.9
5	2nd bending	17.26	18.44	0.51	6.4
6	3rd torsional	22.22	21.63	1.1	2.7
7	4th torsional	28.21	28.42	0.98	0.7
8	2nd bending	37.91	46.73	1.36	18.9
9	2nd in-plane	42.05	36.47	1.8	15.3
10_N	local mode	60.29	-	_	-
10_x	4th bending	-	67.94	2.06	-

Table 5: Comparison of frequencies and damping of the numerical and experimental wing models at $V = 10\text{m/s}$.

B. Appendix B

In order to evaluate the control effort, we evaluate the transfer-function matrix between the disturbance vector $f_d = R(s)(d_1, d_2)^T$ and the commands $u = (u_{LE}, u_{TE})^T$. From Fig.4.b, we have:

$$u = C(s)[I - R(s)C(s)]^{-1} f_d = G_d(s)f_d \qquad (B.1)$$

where $C(s) = F^T s + G^T$ is the receptance based controller, and $r(s)$ is the transfer-function matrix function, relating the control inputs to the control outputs; it includes the dynamics of the subsystems, the amplifiers and the filters as depicted in Fig.4.a.

Eq.(B.1) describes the reaction effort of the controller (i.e. commands to the actuators) to a given disturbance profile. This effort can be evaluated in several ways, one simple way is to consider the mean value of u for a given disturbance vector spectrum. The power spectral density matrix of the commands Φ_u is related to the power spectral density matrix of the disturbances Φ_{f_d} by:

$$\Phi_u(\omega) = G_d(\omega)\Phi_{f_d}(\omega)G_d^*(\omega) \qquad (B.2)$$

where the superscript $*$ stands for the conjugate transpose. Assuming uncorrelated disturbances, with a unit power spectral density, it can be shown that $\Phi_{f_d}(\omega) = I$. Consider now the singular value decomposing (SVD) of the transfer-function matrix $G_d(s)$, such that:

$$G_d(s) = US(s)V^* \qquad (B.3)$$

where the matrices V and U are unity matrices, i.e. $VV^* = I$ and $UU^* = I$; they are also referred to as the input and output matrices, respectively. The matrix $S(s)$ contains the singular values $\sigma_1(s)$ and $\sigma_2(s)$ on its diagonal, with $\sigma_1(s) > \sigma_2(s)$. By substituting Eq.(B.3) into Eq.(B.2), and using the orthonormal property of V, one gets:

$$\Phi_u(\omega) = US^2(s)U^* = \sigma_1^2(\omega)U_1 U_1^* + \sigma_2^2(\omega)U_2 U_2^*. \qquad (B.4)$$

Observe that the control effort power density matrix relies only upon $\sigma_1^2(s)$ and $\sigma_2^2(s)$. The average power of u (mean square) can be obtained by simply integrating $\Phi_u(\omega)$ along the considered frequency bandwidth (in which the disturbance is powerful). Thus to evaluate the control effort, one needs simply to evaluate the area under $\sigma_1^2(s)$ and $\sigma_2^2(s)$ within the frequency band of interest.

VIII. Acknowledgments

IX. References

[1] Mottershead, J. E., and Ram, Y. M., Inverse eigenvalue problems in vibration absorption: passive modification and active control. Mechanical Systems and Signal Processing, vol. 20, No 1, 2006, 5-44.

    doi: 10.1016/j.ymssp.2005.05.006

[2] Ram, Y. M. and Mottershead, J. E., Receptance Method in Active Vibration Control, AIAA Journal, Vol. 45, No. 3, 2007, pp. 562–567.

    doi: 10.2514/1.24349

[3] Roger, K., Airplane math modelling methods via dynamic realization, AGARD CP-228, April 1977.

[4] Roger, K.L., Hodges, G.E. and Felt, L., Active flutter suppression-a flight test demonstration. Journal of Aircraft, vol. 12, No 6, 1975, pp.551-556.

    doi: 10.2514/3.59833

[5] Mukhopadhyay, V., Newsom, J.R. and Abel, I., Reduced order optimal feedback control synthesis for flutter suppression, J Guidance, Control and Dynamics, 5(4), 1982, 389-395

    doi: 10.2514/3.56187

[6] Liebst, B.S., Garrard, W.L. and Adams, W.M., Design of an active flutter suppression system. AIAA Journal of Guidance, Control, and Dynamics, vol. 9, No 1, 1986, pp.64-71.

    doi: 10.2514/3.20068

[7] Andrighettoni, M. and Mantegazza, P., Multi-input/multi-output adaptive active flutter suppression for a wing model. Journal of Aircraft, vol. 35, No. 3, 1998, pp.462-469.

    doi: 10.2514/2.2319

[8] Mukhopadhyay, V., Benchmark Active Control Technology: Part I, Journal of Guidance, Control, and Dynamics, Vol. 23, No. 5, 2000, pp. 913–913.

    doi:10.2514/2.4631

[9] Mukhopadhyay, V., Benchmark Active Control Technology Special Section: Part II, Journal of Guidance, Control, and Dynamics, Vol. 23, No. 6, 2000, pp. 1093–1093.

doi:10.2514/2.4659

[10] Mukhopadhyay, V., Benchmark Active Control Technology Special Section: Part III, Journal of Guidance, Control, andDynamics, Vol. 24, No. 1, 2001, pp. 146–146.

doi:10.2514/2.4693

[11] De Gaspari, A., Ricci, S., Riccobene, L., and Scotti, A., Active aeroelastic control over a multi-surface wing: modelling and wind-tunnel testing, AIAA Journal 47(9), 2009, 1995-2010.

[12] Bendiksen, O. O., Energy Approach to Flutter Suppression and Aeroelastic Control, Journal of Guidance, Control, and Dynamics, Vol. 24, No. 1, 2001, pp. 176–184.

doi:10.2514/2.4699

[13] Zhang, X.T., Wu, Z.G. and Yang, C., New flutter-suppression method for a missile fin with and actuator, J Aircraft, 50(3), 2013, 989-994.

[14] Singh, K.V., Brown, R.N. and Kolonay, R. Receptance-based active aeroelastic control with embedded control surfaces having actuator dynamics, J Aircraft, 53(3), 2016, 830-845.

[15] Ram, Y. M., Mottershead, J. E., Multiple-input active vibration control by partial pole placement using the method of receptances, Mechanical Systems and Signal Processing, Vol. 40, No. 2, 2013, pp. 1–9.

doi: 10.1016/j.ymssp.2013.06.008

[16] Bishop, R. E. D. and Johnson, D. C., The mechanics of vibration. Cambridge University Press, 1960.

doi: 10.1017/S036839310008994X

[17] Weissenburger, J.T., Effect of local modifications on the vibration characteristics of linear systems, Transactions of ASME, Journal of Applied Mechanics, vol. 90, 1968, 327–332.

doi: 10.1115/1.3601199

[18] Sadeghipour, K., Brandon, J. A., and Cowley, A., The receptance modification strategy of a complex vibrating system. International Journal of Mechanical Sciences, 27(11-12), 1985, 841-846.

doi: 10.1016/0020-7403(85)90015-3

[19] Mottershead, J.E., Kyprianou, A., and Ouyang, H., Structural modification, part 1: rotational receptances, Journal of Sound and Vibration, 284(1-2), 2005, 249-265.

[20] Kyprianou, A., Mottershead J.E. and Ouyang, H., Structural modification, part 2: assignment of natural frequencies and antiresonances by an added beam, Journal of Sound and Vibration, 284(1-2), 2005, 267-281.

[21] van der Seijs M.V., de Klerk, D. and Rixen, D.J., General framework for transfer path analysis: History, theory and classification of techniques, Mechanical Systems and Signal Processing, 68-69 (2016) 217–244.

[22] Papatheou, E., Tantaroudas, N. D., Da Ronch, A., Cooper, J. E. and Mottershead, J. E., Active control for flutter suppression: an experimental investigation, in International Forum on Aeroelasticity and Structural Dynamics (IFASD), Bristol June 24-26, 2013, UK, pp. 1-14.

[23] Ghandchi Tehrani, M., Elliott, R. N. R., Mottershead, J. E., Partial pole placement in structures by the method of receptances: Theory and experiments, Journal of Sound and Vibration, Vol. 329, No. 24, 2010, pp. 5017–5035.

   doi : 10.1016/j.jsv.2010.06.018

[24] Xia, M. and Li, S., Active control of structural sound radiation using receptance method. In: INTER-NOISE and NOISE-CON Congress and Conference Proceedings. Institute of Noise Control Engineering, 2017, pp 2218-2225.

[25] Ram, Y. M., Mottershead, J. E., Multiple-input active vibration control by partial pole placement using the method of receptances, Mechanical Systems and Signal Processing, Vol. 40, No. 2, 2013, pp. 1–9.

   doi: 10.1016/j.ymssp.2013.06.008

[26] Singh, K. V., McDonough, L. A., Kolonay, R., and Cooper, J. E., Receptance-based active aeroelastic control using multiple control surfaces. Journal of Aircraft, vol. 51, No 1, 2014, 335-342.

   doi: 10.2514/1.C032183

[27] C. Zhen, S. Jiffri, D.-C. Li, J.-W. Xiang and J.E. Mottershead, Feedback linearisation of nonlinear vibration problems: a new formulation by the method of receptances, *Mechanical Systems and Signal Processing*, 98, 2018, 1056-1068.

 [28] Lisitano, D., Jiffri, S., Bonisoli, E., and Mottershead, J. E., Experimental feedback linearisation of a non-smooth nonlinear system by the method of receptances. Mathematics and Mechanics of Solids, 2017, p. 1081286517744601.

   doi: 10.1177/1081286517744601

 [29] Livne, E., Aircraft Active Flutter Suppression: State of the Art and Technology Maturation Needs, Journal of Aircraft, vol. 55, No. 1, 2018, pp. 410–452.

   doi: 10.2514/1.C034442

[30] S. Fichera , S. Jiffri and Mottershead, J. E., Design and wind tunnel test of a MODular aeroelastic FLEXible wing (MODFLEX), International Conference on Noise and Vibration Engineering (ISMA2016), Leuven 19-21 Sept. 2016, Belgium.

[31] Peeters, B., Lowet, G., Van Der Auweraer, H. and Leuridan, J., A New Procedure for Modal Parameter Estimation, Sound and Vibration, Vol. 38, 2004, pp. 24–28.